Catalysis Science & Technology

Accepted Manuscript

ROYAL SOCIETY OF CHEMISTRY

www.rsc.org/catalysis

Cite this: DOI: 10.1039/c0xx00000x

www.rsc.org/xxxxxx

ARTICLE TYPE

Ceria-zirconia modified MnO_x catalysts for gaseous elemental mercury oxidation and adsorption

Deshetti Jampaiah[a,b], Samuel J. Ippolito[b], Ylias M. Sabri[b], James Tardio[b], P. R. Selvakannan[b], Ayman Nafady[c,d], Benjaram M. Reddy*[a] and Suresh K. Bhargava*[b]

Received (in XXX, XXX) Xth XXXXXXXXX 20XX, Accepted Xth XXXXXXXXX 20XX
DOI: 10.1039/b000000x

Abstract A series of MnO_x/CeO_2 (Mn/Ce), MnO_x/ZrO_2 (Mn/Zr), and $MnO_x/Ce_{0.75}Zr_{0.25}O_2$ (Mn/CZ) catalysts prepared by an impregnation method were tested for their ability to catalyse oxidation of Hg^0 at relatively low temperature (423 K). Various characterization techniques, namely, Brunauer–Emmett–Teller (BET) surface area, X-ray diffraction (XRD), Raman spectroscopy (RS), X-ray photoelectron spectroscopy (XPS), and H_2-temperature programmed reduction (H_2-TPR) were employed to understand the structural, surface, and redox properties of the prepared catalysts. Specific aspects of the catalysis of Hg^0 oxidation that were investigated included the influence of MnO_x loading (5, 15, and 25 %) and the influence of HCl and O_2. Among the catalysts tested, the15Mn/CZ catalyst achieved the highest Hg^0 oxidation performance (~ 83 % conversion of Hg^0 to Hg^{2+}) in the presence of HCl and O_2. The higher activity of the 15 Mn/CZ catalyst was most likely due to the presence of more oxygen vacancies, enhanced $Mn^{4+}/Mn^{4+}+Mn^{3+}+Mn^{2+}$ ratio and more surface adsorbed oxygen, which are proved by XRD, BET, Raman, and XPS. H_2-TPR results also show that the strong interaction between $Ce_{0.75}Zr_{0.25}O_2$ support and MnO_x improved redox properties significantly while compared to pure CeO_2 and ZrO_2 supported MnO_x catalysts.

1. Introduction

Mercury (Hg) emissions are a global concern because of the potential risks Hg poses to human health and the environment.[1] In particular, it can affect human health by acting as a neurotoxin, harming the human development system. Furthermore, long term exposure to methyl mercury ($(CH_3)_2Hg$) can damage the heart, kidneys, lungs, and immune system of people from all age groups. Coal-fired power plants are one of the major man-made sources of mercury emissions. Three general forms of Hg species are generated during coal combustion, namely, elemental mercury (Hg^0), oxidised mercury (Hg^{2+}), and particulate mercury (Hg_p).[2, 3] Existing flue gas treatment technologies in coal-fired power plants such as wet scrubbers, electrostatic precipitators (ESP), and fabric filters (FF) can efficiently remove both Hg^{2+} -and Hg_p from coal-fired flue gas. The Hg^0 present in the flue gas is however very difficult to control due to its high volatility and low solubility in water.[4-6] Moreover, Hg^0 is the predominant-specie in flue gas, accounting for 66–94 % of the total mercury emissions.[7] Based on the potential adverse effects of Hg^0, there is significant interest in the development of process for removing this from flue gas.

In recent years, catalytic conversion of Hg^0 to its oxidised form, Hg^{2+} has attracted prominent interest because the converted Hg^{2+} can be easily removed by wet flue gas desulfurization (WFGD) technology.[8, 9] Various transition metal oxides such as TiO_2, Cu_2O, MnO_x, Fe_2O_3, and V_2O_5 have been effectively examined for Hg^0 removal from flue gas through catalytic oxidation and adsorption process.[10-16] Among them, manganese oxide has received significant interest based on a combination of some initial promising results and its relatively low cost as compared to noble metals.[10, 17, 18] Unsupported MnO_x catalysts however have been shown to not perform well in catalytic oxidation of Hg^0–this was reported to be due to their larger particle sizes.[19] Different supports such as Al_2O_3, TiO_2, and activated carbons have been used to enhance the catalytic performance of MnO_x catalysts. For example, Qiao et al.[8] reported that MnO_x/Al_2O_3 material show significant Hg^0 oxidation efficiency (> 80 %) after 2 hours in the presence of HCl (20 ppm) under the following conditions (Hg^0_{inlet}= 180 µg/m^3, T = 623 K). Ji et al.[20] prepared a novel MnO_x/TiO_2 catalyst that exhibited > 90 % catalytic activity for Hg^0 oxidation. The significant catalytic performance of MnO_x has reported to be due

[a]RMIT-IICT Joint Research Centre, CSIR-Indian Institute of Chemical Technology, Uppal Road, Hyderabad – 500 607, India E–mail addresses: bmreddy@iict.res.in; mreddyb@yahoo.com Phone: +91 40 2719 3510; fax: +91 40 2716 0921.
[b]Centre for Advanced Materials & Industrial Chemistry (CAMIC), School of Applied Sciences, RMIT University, GPO BOX 2476, Melbourne–3001, Australia. E-mail: suresh.bhargava@rmit.edu.in; Tel: +61 3 9925 3365
[c]Chemistry Department, College of Science, King Saud University, Riyadh, Saudi Arabia
[d]Chemistry Department, Faculty of Science, Sohag University, Sohag 82524, Egypt

†Electronic supporting Information available: Experimental setup for Hg^0 removal, Hg^0 removal blank experiments, and H_2 consumption values of the investigated catalysts.

to its multiple oxidation states (Mn^{4+}/Mn^{3+}) as well as various types of labile oxygen species.[21, 22] Whilst MnO_x based catalysts have been shown to achieve promising results to date there are some significant drawbacks that have been reported for these catalysts. Firstly it has been reported that these catalysts have low resistance to sulphur dioxide (SO_2) poisoning (where SO_2 is a common component of coal fired flue gas).[23] Moreover very high HCl concentrations (in excess of those commonly found in coal fired flue gas) have been necessary in order to obtain very high Hg^0 oxidation efficiencies over MnO_x based catalysts supported on TiO_2 and/or Al_2O_3 supports.[24]

In this study the ability of a range of MnO_x based materials to catalyse the oxidation of Hg^0 was investigated in presence of low HCl concentration (10 ppm). The support used in this study (CeO_2–ZrO_2) were chosen based on its successful application in several industrial catalytic process such as selective catalytic reduction (SCR) of NO_x with NH_3, water gas shift (WGS) reactions, and soot oxidation reactions.[25-27] Furthermore, CeO_2–ZrO_2 based materials not only act as good supports but also as co-catalyst by providing active oxygen atoms to the dispersed active component in various oxidation reactions.[28] Hence, the combination of MnO_x and CeO_2–ZrO_2 can benefit the application of manganese-based oxides in Hg^0 oxidation. Therefore, to improve the Hg^0 removal performances of Mn-based catalysts, different weight percentages of MnO_x was deposited on CeO_2–ZrO_2 support by employing an impregnation method. The synthesized catalysts were tested towards Hg^0 removal under simulated flue gas conditions (HCl and O_2) at a low operating temperature of 423 K. The effect of different loading amounts of MnO_x on CeO_2–ZrO_2 support towards Hg^0 oxidation and adsorption performances was also clearly discussed.

2. Experimental section

2.1 Catalysts preparation

$Ce_{0.75}Zr_{0.25}O_2$ was prepared by a co-precipitation method using aqueous ammonia (aq.NH_3) as the precipitating agent. The precursors used in the synthesis were $Ce(NO_3)_3$•$6H_2O$ (*Aldrich, AR grade*) and $ZrO(NO_3)_2$•xH_2O (*Aldrich, AR grade*). The molar ratios of Zr/(Ce+Zr) over the $Ce_{0.75}Zr_{0.25}O_2$ support were 25 %. In a typical synthesis, the 0.015 mole (6.513 g) of Ce-nitrate and 0.005 mole (1.156 g) of Zr-oxynitrate precursors were dissolved with stirring in 200 mL of distilled water for 30 minutes. Then, aqueous NH_3 (25 % w/v) was added dropwise with vigorous stirring to attain a pH of 9. Subsequently, the precipitate was washed three times with distilled water and ethanol to remove NH_4^+ and NO_3^- impurities. The collected product was dried at 353 K in an oven for overnight and then calcined at 773 K for 5 h.

$MnO_x/Ce_{0.75}Zr_{0.25}O_2$ materials were prepared by an impregnation method using $Mn(NO_3)_2$•$4H_2O$ (*Merck, AR grade*) and $Ce_{0.75}Zr_{0.25}O_2$ (see previous paragraph). The molar ratios of Mn/(Ce+Zr) over the $MnO_x/Ce_{0.75}Zr_{0.25}O_2$materials were 5, 15, and 25 %. The required amount of Mn-nitrate precursor was dissolved in distilled water followed by adding the $Ce_{0.75}Zr_{0.25}O_2$ support to the solution. Aqueous ammonia was then added slowly until the precipitation was complete (giving a final solution pH of 9). The obtained product was washed three times with distilled water and ethanol and dried at 353 K for overnight. The dried sample was calcined at 773 K for 5 h. The as-prepared catalysts $Ce_{0.75}Zr_{0.25}O_2$, 5 % $MnO_x/Ce_{0.75}Zr_{0.25}O_2$,15% $MnO_x/Ce_{0.75}Zr_{0.25}O_2$, and 25% $MnOx/Ce_{0.75}Zr_{0.25}O_2$ were designated as CZ, 5Mn/CZ, 15Mn/CZ, and 25Mn/CZ, respectively. CeO_2 and ZrO_2 supports were prepared by precipitation method using their respective salts. Then, MnO_x/CeO_2 (Mn/Ce) and MnO_x/ZrO_2 (Mn/Zr) catalysts were prepared by a similar method as that used to prepare Mn/CZ catalysts.

2.2 Catalysts characterization

The N_2 specific BET surface areas and pore size distributions were measured on a Micromeritics (ASAP 2000) analyzer. Prior to analysis, approximately 100–200 mg of sample was degassed under vacuum at 523 K for 10 h. The specific surface area (S_{BET}) of each sample was calculated by the multipoint BET method and average pore size was calculated by the Barrett-Joyner-Halenda (BJH) method from the N_2 desorption branches of the isotherm.

Powder XRD measurements were performed on a Rigaku Multiflex diffractometer with a Cu Kα (0.15418 nm) radiation source. The 2θ values in the range of 10–80° were collected with a 0.021° step size. The obtained diffraction patterns were matched with the international centre for diffraction data-powder diffraction file (ICDD-PDF). The lattice parameters (*a*) were measured by XRD refinement and average crystallite sizes (D) were calculated using Sherrer's equation.

Raman measurements were carried out at room temperature with a DILORXY spectrometer using an Ar^+ ion (Spectra Physics) laser source (632 nm).

XPS measurements were made on a K-α spectrometer (Thermo scientific) at room temperature under ultra-high vacuum (10^{-8} Pa). The monochromatic Al-Kα (1486.7 eV) radiation source was used as the excitation source. All binding energies of the samples were calibrated using the reference carbon (C 1s) peak at 285 eV. The spectra were fitted with the Avantage software and Shirley background was used for fitting all levels.

H_2–TPR experiments were done on an automated AutoChem. II-2720 (Micromeritcs) chemisorption analyser equipped with a thermal conductivity detector (TCD). Before analysis, the catalyst (approx. 50 mg) was preheated with a pure helium gas in a quartz glass reactor with a flow rate of 20 mL/min for 30 minutes up to 573 K and then cooled down to room temperature (RT) by purging Argon gas. Then, the sample was exposed to a reduction agent, 5 % (v/V) of H_2 at a flow rate of 20 mL/min from 298 to 1073 K with ramping time of 50 K/min.

2.2 Catalytic activity test

The Hg^0 removal efficiencies of the catalysts were tested using a bench scale catalytic reactor as shown in supporting information, Fig. S1. The reactor consisted of a Hg^0 vapour generator, HCl

vapour generator, temperature-controlled quartz reactor and mercury speciation trapping system. The typical simulated flue gas used in the study was 10 ppm HCl, and 3 % O_2 with the balance being dry N_2. The total flow rate of all gases combined was maintained at 200 mL/min throughout the experiments using mass flow controllers (John Morris Scientific). A mercury permeation device (VICI, Metronics Inc.) was used to generate Hg^0 vapour generator at a constant concentration of ~320 µg/m^3 by using a fixed temperature of 313 K at the generator. It must be noted that an online mercury analyzer is not employed in this study. Therefore a Hg^0 vapor concentration of ~320 µg/m^3 was purposefully used in this study as the higher mercury levels in our chemical speciation traps provided a more accurate (less error) mass balance for the mercury in the system and therefore a more realistic catalytic oxidation performance of the developed catalysts. The HCl vapour was also generated using a HCl permeation device (VICI, Metronics Inc.), which was placed inside an in-house built Teflon cell. The produced Hg^0 and HCl vapours from the generators were passes to the reaction chamber with dry N_2 carrier gas by maintaining a constant temperature of 363 K around the pipe lines. For Hg^0 removal experiments, approximately 0.4 g of the catalyst was loaded into quartz reactor (Ø = 1 cm) and the reaction temperature was maintained at 423 K for the entire reaction period of 16 h. In each test, quartz wool was used as a support for the catalyst. Previous studies have confirmed that the quartz wool has no impact on Hg^0 removal under the conditions used in this study.[29]

The elemental and the converted oxidised mercury were measured quantitatively using a modified Ontario Hydro Method (OHM),[30, 31] in which KCl (0.01 M) and $KMnO_4/H_2SO_4$ (20 mg/L) impinger solutions were used in the train of traps as mercury absorbing media. According to OHM, the elemental mercury (Hg^0) was captured by $KMnO_4$ solution, whereas oxidised mercury (Hg^{2+}) was absorbed by KCl solution. In order to maintain full mass balance in the experiment, the adsorbed mercury (Hg_{ads}) on the catalyst surface was measured using acid-digestion experiments, in which a known amount of sample was digested by aqua regia (1:3 Conc. HNO_3 and HCl) and kept overnight at room temperature. Then, the quantitative amount of Hg^0, Hg^{2+}, and Hg_{ads} were determined using an inductive coupled plasma-mass spectrometry (ICP-MS) from Agilent Technologies (7700x series) with an ASX 520 series autosampler. In order to ensure the accuracy of the experimental methodology, various quality controls were followed which include mercury specific analysis settings, validating the data, using multiple internal standards and using collision analysis mode where necessary. In all of the experiments, the inlet, oxidised, adsorbed, and outlet mercury were represented as Hg^0_{inlet}, Hg_{oxi}, Hg_{ads}, and, Hg^0_{outlet}, respectively. The amount of Hg^0_{inlet} was determined by performing 10 experiments without any catalyst as shown in the supporting information, Fig. S2. The total Hg is the sum of Hg_{ads}, Hg_{oxi}, and Hg^0_{outlet}, which is also equal to Hg^0_{inlet} (~61±2 ppbv in 16 h), thereby confirming that a full mass balance is attained in all the experiments. The Hg^0 removal efficiency can be defined as the sum of total of Hg^0 oxidation efficiency (E_{oxi}, %) and Hg^0 adsorption efficiency (E_{ads}, %), which were described in the following equations.

$$E_{oxi}\,(\%) = \frac{Hg_{oxi}}{Hg^0_{inlet}} \times 100 \quad (1)$$

$$E_{ads}\,(\%) = \frac{Hg_{ads}}{Hg^0_{inlet}} \times 100 \quad (2)$$

3. Results and discussion

3.1 Characterization studies

3.1.1 BET surface area

The N_2 BET isotherms obtained for Mn/Zr, Mn/Ce, 5Mn/CZ, 15Mn/CZ, 25Mn/CZ, and CZ catalysts are shown in Fig. 1. The Mn/Ce and Mn/Zr samples show type III adsorption isotherm, whereas Mn/CZ and CZ samples display type IV adsorption isotherm, which is indicating that all catalysts were mesoporous in nature.[32] The values of specific BET surface area, average pore diameter, and total pore volume of each catalyst are compiled in Table 1. The specific surface area of the Mn/Ce and Mn/Zr catalysts were found to be 36.4 and 42.6 m^2 g^{-1}, respectively. The CZ support had the highest specific surface area (84 m^2 g^{-1}) of all the catalysts. In case of CZ supported MnO_x catalysts, the surface areas decreased and the values were in the range of 82.6–78.9 m^2 g^{-1}. It can be concluded that the dispersed MnO_x particles might decrease the surface area by occupying the free pores of CZ support. From Table 1, it can also be observed that the Mn/CZ catalysts have larger pore volumes and smaller pore diameters than the Mn/Ce and Mn/Zr catalysts.

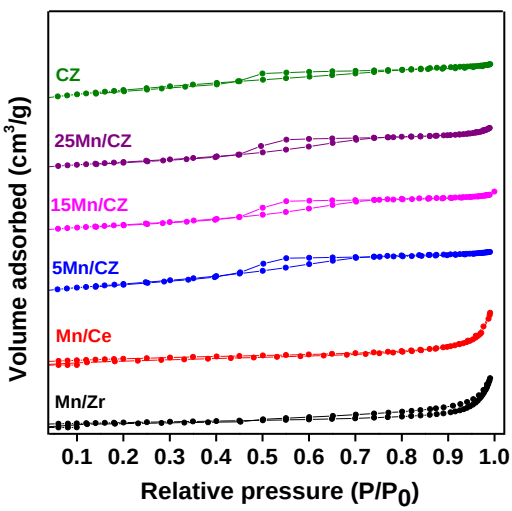

Fig.1 Nitrogen adsorption-desorption isotherms of MnO_x/ZrO_2 (Mn/Zr), MnO_x/CeO_2 (Mn/Ce), 5% $MnO_x/Ce_{0.75}Zr_{0.25}O_2$ (5Mn/CZ), 15% $MnO_x/Ce_{0.75}Zr_{0.25}O_2$ (15Mn/CZ), 25% $MnO_x/Ce_{0.75}Zr_{0.25}O_2$ (25Mn/CZ), and $Ce_{0.75}Zr_{0.25}O_2$ (CZ) catalysts.

Table 1 The specific BET surface area, pore diameter, and pore volume of MnO_x/CeO_2 (Mn/Ce), MnO_x/ZrO_2 (Mn/Zr), $Ce_{0.75}Zr_{0.25}O_2$ (CZ), 5% $MnO_x/Ce_{0.75}Zr_{0.25}O_2$ (5Mn/CZ), 15% $MnO_x/Ce_{0.75}Zr_{0.25}O_2$ (15Mn/CZ), and 25% $MnO_x/Ce_{0.75}Zr_{0.25}O_2$ (25Mn/CZ) catalysts.

Catalyst	BET surface area (m^2/g)	Average pore diameter (nm)	Total pore volume (cm^3/g)
Mn/Ce	36.4	15.9	0.03
Mn/Zr	42.6	12.1	0.02
CZ	84	6.2	0.08
5Mn/CZ	82.6	4.8	0.11
15Mn/CZ	80.3	4.5	0.15
25Mn/CZ	78.9	4.7	0.13

3.1.2 XRD analysis

The powder XRD patterns of the Mn/Zr, Mn/Ce, Mn/CZ and CZ catalysts are shown in Fig. 2. Diffraction lines consistent with CeO_2 and ZrO_2 phases were observed in the Mn/Ce and Mn/Zr catalysts, respectively. Manganese oxide (MnO_2 and Mn_2O_3) phases were also present in both the Mn/Ce and Mn/Zr catalysts based on the diffraction patterns obtained for these catalysts. For the CZ catalyst, the diffraction lines in the pattern obtained were consistent with the catalyst having a cubic fluorite structured CeO_2 (ICDD-PDF 34-0394).[5,33,34] Furthermore, these diffraction lines were slightly shifted towards higher 2θ angles compared to those observed in the pure CeO_2 supported MnO_x catalyst. The shifting observed for the CZ catalyst was most likely due to the doping of Zr^{4+} into fluorite structured CeO_2 lattice.[35,36] The XRD patterns obtained for Mn/CZ catalysts were similar to the pattern obtained for the CZ support. Interestingly, the XRD patterns for the catalysts with 5 and 15 % Mn loading did not have any diffraction lines related to manganese oxides, whereas the 25Mn/CZ catalyst had diffraction lines consistent with MnO_2 and Mn_2O_3 phases along with CeO_2. It shows that with increasing Mn loading (up to 25 %), different Mn-oxide phases were observed most likely due to crystalline MnO_x phases. On the other hand, at lower loading up to 15 %, the MnO_x is also most likely amorphous and/or well dispersed over CZ support. The average crystallite sizes (*D*) of catalysts are calculated by Debye-Sherrer equation and illustrated in Table 2. The obtained CeO_2 crystallite sizes of Mn/CZ catalysts are smaller than Mn/Ce catalyst. The lattice parameters were also calculated and are given in Table 2. The CZ and Mn/CZ catalysts show smaller lattice parameters, 5.35 and 5.31 Å, respectively, while compared to pure CeO_2 support (5.42 Å) due to lattice contraction. This observation also provides an evidence for shifting of diffraction lines towards higher angle side for the Mn/Ce catalyst.

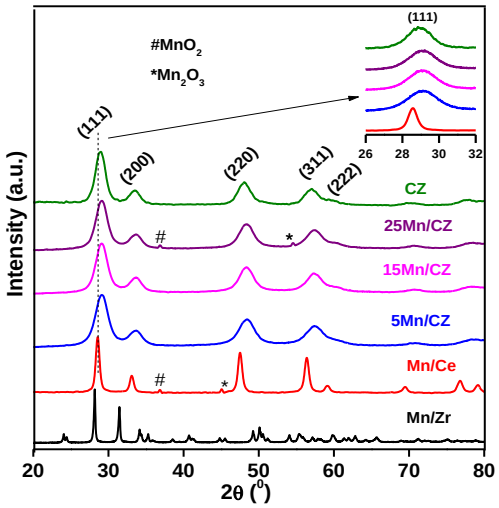

Fig. 2 Powder XRD patterns of MnO_x/ZrO_2 (Mn/Zr), MnO_x/CeO_2 (Mn/Ce), 5% $MnO_x/Ce_{0.75}Zr_{0.25}O_2$ (5Mn/CZ), 15% $MnO_x/Ce_{0.75}Zr_{0.25}O_2$ (15Mn/CZ), 25% $MnO_x/Ce_{0.75}Zr_{0.25}O_2$ (25Mn/CZ), and $Ce_{0.75}Zr_{0.25}O_2$ (CZ) catalysts.

Table 2 The crystallite size, lattice parameter, and Raman full width half maxima (FWHM) values of MnO_x/CeO_2 (Mn/Ce), $Ce_{0.75}Zr_{0.25}O_2$ (CZ), 5% $MnO_x/Ce_{0.75}Zr_{0.25}O_2$ (5Mn/CZ), 15% $MnO_x/Ce_{0.75}Zr_{0.25}O_2$ (15Mn/CZ), and 25% $MnO_x/Ce_{0.75}Zr_{0.25}O_2$ (25Mn/CZ) catalysts.

Catalyst	Crystallite size (nm)[a]	Lattice parameter (Å)[b]	Raman FWHM (cm^{-1})[c]
Mn/Ce	14.39	5.42	14.5
CZ	5.85	5.35	49.8
5Mn/CZ	4.26	5.31	87.6
15Mn/CZ	4.68	5.31	97.2
25Mn/CZ	4.58	5.31	73.4

[a,b]calculated from (111) lattice plane from XRD
[c]measured from Raman F_{2g} peak

3.1.3 Raman analysis

Raman spectra were obtained for the Mn/Ce, Mn/CZ, and CZ catalysts in order to investigate any differences in the Ce–O bonding between the respective catalysts (Fig. 3). The Mn/Ce catalyst provides typical CeO_2 Raman spectra with an intense band at ~ 461 cm^{-1}, which can be attributed to the F_{2g} Raman active mode of the cubic fluorite structure with a symmetrical vibration mode of oxygen atoms around each Ce^{4+} cation.[37,38]

Interestingly, the CZ support and Mn/CZ catalysts displayed a Raman band at around 475 cm^{-1}, which is significantly higher than that obtained for Mn/Ce catalyst.[27] As the position and width of Raman bands depend on several factors such as crystallite growth and particle sizes, the aforementioned F_{2g} band position indicates a significant difference in the Ce–O structure when present in CZ and Mn/CZ catalysts as compared to the Mn/Ce catalyst.[35,39,40] As shown in Table 2 (XRD), the average crystallite sizes of the Mn/CZ catalyts decreased with increasing Mn loading, with the values being in the range of 4.68–4.26 nm compared to Mn/Ce catalyst (14.39 nm). Furthermore, the full width half maxima (FWHM) of the peak at 475 cm^{-1} in the CZ and Mn/CZ catalysts were significantly broader compared to the Mn/Ce catalyst. These results imply that the decrease in crystallite sizes causes to enhance width of F_{2g} Raman band. Additionally, for CZ catalyst, the two weak Raman peaks at 278 and 623 cm^{-1}, can be due to the Raman inactive transverse and longitudinal optical phonon modes, respectively.[41,42] Particularly, the peak at 623 cm^{-1} can also be attributed to oxygen vacancies (O_v) in the ceria lattice due to the incorporation of Zr^{4+} into CeO_2.[35] The Mn/CZ catalysts also show a O_v band at 623 cm^{-1}, but as the Mn loading increases to 15 %, the O_v intensity increased. However, for 25Mn/CZ catalyst, the O_v intensity disappeared when the MnO_x loading reaches to 25 %. Additionally, the peaks related to MnO_2 and Mn_2O_3 appeared for 25Mn/CZ catalyst. It clearly indicates that the optimum loading of 15 % MnO_x on CZ support could provide the well dispersion of MnO_x, which is also supported by XRD results.

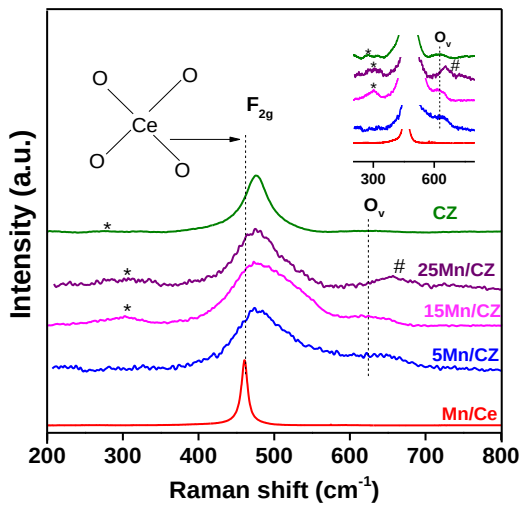

Fig. 3 Raman spectra of MnO_x/CeO_2 (Mn/Ce), 5 % $MnO_x/Ce_{0.75}Zr_{0.25}O_2$ (5Mn/CZ), 15% $MnO_x/Ce_{0.75}Zr_{0.25}O_2$ (15Mn/CZ), 25 % $MnO_x/Ce_{0.75}Zr_{0.25}O_2$ (25Mn/CZ), and $Ce_{0.75}Zr_{0.25}O_2$ (CZ) catalysts.

3.1.4 XPS analysis

XPS analysis was employed to determine the chemical state and the relative proportion of elements present in the catalysts. Fig. 4a shows the Mn 2p XPS spectra of fresh Mn/Zr, Mn/Ce, and 15Mn/CZ catalysts. As for Mn 2p, there are two peaks appeared at ~641 and 653 eV, which can be attributed to spin-orbit doublet of Mn $2p_{3/2}$ and Mn $2p_{1/2}$, respectively. The Mn $2p_{3/2}$ peak of Mn/Zr, Mn/Ce, and 15Mn/CZ catalysts can be separated by denconvolution into three peaks at ~ 640.2–640.4, ~ 641.4–642.2, and ~ 643.1–644.2 eV, which can be attributed to Mn^{2+}, Mn^{3+}, and Mn^{4+}, respectively.[43,44] Earlier reports have shown that a high Mn^{4+} concentration would lead to higher catalytic performance in oxidation reactions.[3,26,45,46] Thus, the relative content of Mn^{4+} to total Mn concentration of fresh catalysts was calculated and illustrated in Table 3. It was found that the 15Mn/CZ catalyst show higher Mn^{4+} content (25.98 %) while compared to Mn/Zr (17.73 %) and Mn/Ce (21.52 %).

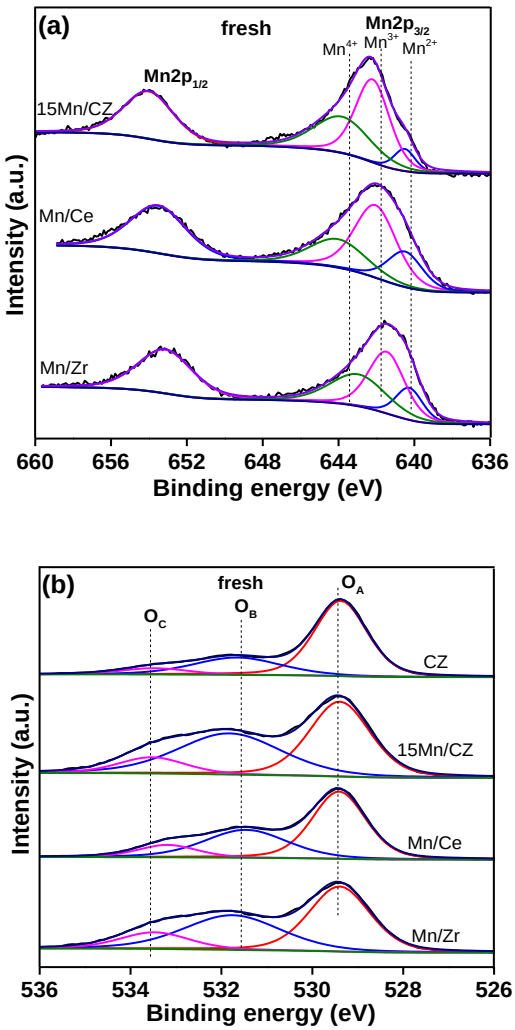

Fig. 4 (a) Mn 2p and (b) O 1s XPS spectra of MnO_x/ZrO_2 (Mn/Zr), MnO_x/CeO_2 (Mn/Ce), 15% $MnO_x/Ce_{0.75}Zr_{0.25}O_2$ (15Mn/CZ), and $Ce_{0.75}Zr_{0.25}O_2$ (CZ) catalysts.

Table 3 Surface atomic ratios of MnO_x/ZrO_2 (Mn/Zr), MnO_x/CeO_2 (Mn/Ce), 15% $MnO_x/Ce_{0.75}Zr_{0.25}O_2$ (15Mn/CZ), and $Ce_{0.75}Zr_{0.25}O_2$ (CZ) catalysts.

Catalyst	$\frac{Ce^{4+}}{Ce^{3+}+Ce^{4+}}$ (%)	$\frac{Mn^{4+}}{Mn^{4+}+Mn^{3+}+Mn^{2+}}$ (%)	O atomic concentration (%)		
			O_A	O_B	O_C
Mn/Zr	-	17.73	60.76	28.21	11.03
Mn/Ce	84.86	21.52	61.51	28.75	9.74
CZ	81.54	-	65.2	26.4	8.4
Fresh 15Mn/CZ	79.46	25.98	58.39	35.31	6.3
Spent 15Mn/CZ	76.23	12.48	52.3	32.3	15.4

The O 1s XPS spectra of fresh Mn/Zr, Mn/Ce, 15Mn/CZ, and CZ catalysts were also analysed as shown in Fig. 4b. The O 1s XPS spectra clearly showed three different oxygen species were present on the surface of the catalysts. The peaks at lower binding energy (~529.2 eV) can be attributed to lattice oxygen (represented as O_A), while the peaks at ~531.4 eV can be ascribed to weakly surface adsorbed oxygen and/or hydroxyl groups (represented as O_B). Lastly, the peak at ~533.6 eV can be attributed to oxygen from water and/or carbonates (represented as O_C).[47,48] The relative concentrations of three oxygen species were calculated by deconvoluting the O 1s spectra and the values are discussed in Table 3. It was clear that the surface adsorbed oxygen of 15Mn/CZ catalyst is higher than that of other catalysts and the order was 15Mn/CZ > Mn/Ce > Mn/Zr > CZ. The surface adsorbed oxygen from both dispersed MnO_x and CZ support could be contributed to appearance of more adsorbed oxygen on the 15Mn/CZ catalysts. Several other groups have reported that the high percentages of adsorbed oxygen leads to higher lattice oxygen mobile, thereby potentially enhancing catalytic oxidation performance.[49-51] Thus, the relative high percentage of O_B on the surface of 15Mn/CZ catalyst could be responsible for enhancing Hg^0 oxidation performances while compared to other catalysts in the study.

The Ce 3d XPS profiles of fresh Mn/Ce, 15Mn/CZ, and CZ catalysts were also shown in Fig. 5a. The Ce 3d XPS spectra composed of eight peaks, namely, u, u', u'', u''', v, v', v'', v''' which can be attributed to four pairs of $3d_{5/2}$ and $3d_{3/2}$ spin-orbit doublets.[3,52] The u, u'', u''', v, v'', v''' represents Ce^{4+}, whereas u' and v' belong to Ce^{3+} state. It shows the co-existence of both 3+ and 4+ oxidation states of Ce. In order to know the relative proportion of Ce amount in CZ, Mn/Ce, and 15 Mn/CZ catalysts, the peaks were deconvoluted and the ratios of $Ce^{4+}/Ce^{3+}+Ce^{4+}$ are summarized in Table 3. Compared to Mn/Ce and CZ catalysts, the Ce^{4+} concentration of 15Mn/CZ catalyst was lower and it indicates that the loading of MnO_x enhanced the Ce^{3+} content of CZ catalyst. The presence of Ce^{3+} ions in the catalyst could create charge imbalance, thereby appearance of more surface adsorbed oxygen species (i.e, O_2^{2-}, O^-, O_2^-) on the surface.[50] Therefore, it is believed that the high content of Ce^{3+} ions associated with adsorbed oxygen species on the surface of 15Mn/CZ catalyst could enhance Hg^0 removal efficiencies.

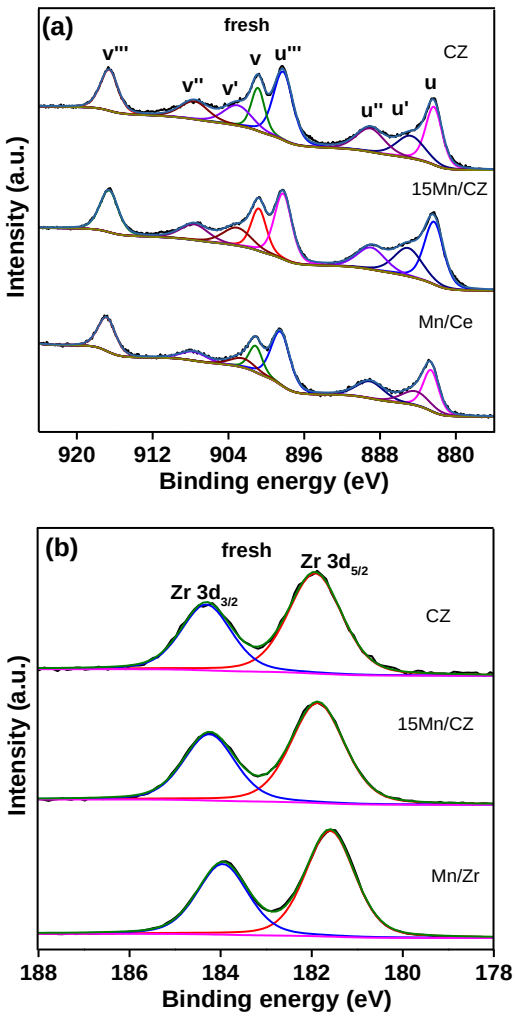

Fig. 5 (a) Ce 3d and (b) Zr 3d XPS spectra of MnO_x/ZrO_2 (Mn/Zr), MnO_x/CeO_2 (Mn/Ce), 15% MnOx/$Ce_{0.75}Zr_{0.25}O_2$ (15Mn/CZ), and $Ce_{0.75}Zr_{0.25}O_2$ (CZ) catalysts.

The Zr 3d XPS spectra of fresh Mn/Zr, 15Mn/CZ, and CZ catalysts were shown in Fig. 5b. As shown, the peak appeared in the range of 181.5–181.9 eV (Zr $3d_{5/2}$) can be attributed to the sole presence of Zr^{4+} in the samples.[41]

3.1.5 H_2-TPR analysis

The redox properties of the CZ, Mn/Zr, Mn/Ce, and 15Mn/CZ catalysts were investigated by a H_2-TPR technique and demonstrated in Fig. 6. In order to compare the redox property of ceria-based catalysts, the pure CeO_2 TPR pattern also included.

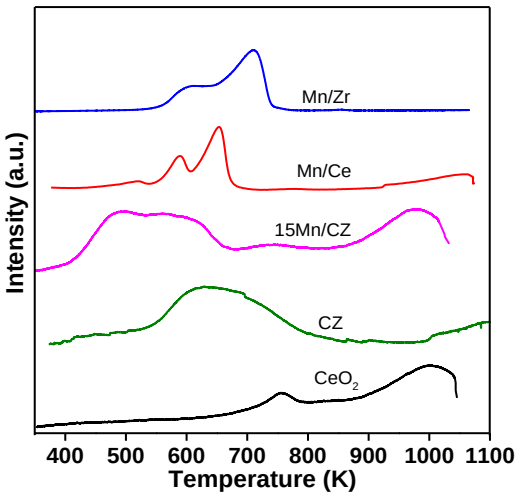

Fig. 6 H_2-TPR profiles of CeO_2, $Ce_{0.75}Zr_{0.25}O_2$ (CZ), 15% $MnO_x/Ce_{0.75}Zr_{0.25}O_2$ (15Mn/CZ), MnO_x/CeO_2 (Mn/Ce), and MnO_x/ZrO_2 (Mn/Zr) catalysts.

As can be seen from Fig. 6, pure CeO_2 shows two reduction peaks at 756 and 1007 K, which can be attributed to surface and bulk reduction of Ce^{4+} to Ce^{3+}, respectively. On the other hand, the Mn/Zr catalyst had two reduction peaks at 602 (T_1), and 711 K (T_2).[53] The primary peak at low temperature can be attributed to the reduction of MnO_2 to Mn_2O_3, whereas the high temperature peak is due to reduction of Mn_2O_3 to Mn_3O_4. The Mn/Ce catalyst exhibits three reduction peaks (519 K (T_1), 588 K (T_2), and 653 K (T_3)) along with bulk reduction of CeO_2 at 1061 K. The third peak at 653 K can be attributed to the combined reduction of Mn_3O_4 to MnO and surface Ce^{4+} to Ce^{3+} species. The CZ support exhibit reduction peaks at around 750 and 1006 K, which are similar to pure CeO_2.[54,55] After loading 15 % of MnO_x on CZ support, the first two reduction peaks appeared at lower temperatures (494 (T_1) and 565 (T_2)) while compared to Mn/Ce and Mn/Zr catalysts. It indicates that the dispersion of MnO_x on CZ support enhanced the redox behaviour of MnO_x while compared to pure metal oxides (CeO_2 and ZrO_2) supports. The bulk reduction temperature peak of CeO_2 also shifted to lower temperature indicates the interaction between CZ support and dispersed MnO_x nanoparticles. Furthermore, the different types of reduction peaks confirm the existence of various manganese oxidation species such as Mn^{2+}, Mn^{3+}, and Mn^{4+}, which is also supported by XPS results. Table S1 (supporting information) shows the H_2 consumption values of CZ, Mn/Zr, Mn/Ce, and 15Mn/CZ catalysts. The 15Mn/CZ catalyst displayed the highest H_2 consumption among all the catalysts and the order was 15Mn/CZ > CZ > Mn/Ce > Mn/Zr. It is well reported that the lower temperature reduction peaks indicates better redox properties and higher H_2 consumption could enhance catalytic activity.[25, 45] Therefore, it is believed that CZ supported MnO_x catalyst could enhance Hg^0 removal performance.

3.2 Hg^0 removal studies

Catalytic oxidation and adsorption of gaseous Hg^0 was investigated using the catalysts described in the preceding sections. The removal efficiency is the sum of E_{oxi} (the amount of gaseous phase Hg (II) that exited the reactor and was captured in the KCl impinger) and E_{ads} (the amount of Hg adsorbed to the catalytic material after the testing period).The influence of HCl and O_2 on catalytic oxidation and/or adsorption of Hg^0 were studied under the following conditions: 320 μg/m^3 of Hg^0, 10 ppm HCl, 3 % O_2, T = 423 K, and reaction time= 16 h.

3.2.1 Effect of HCl

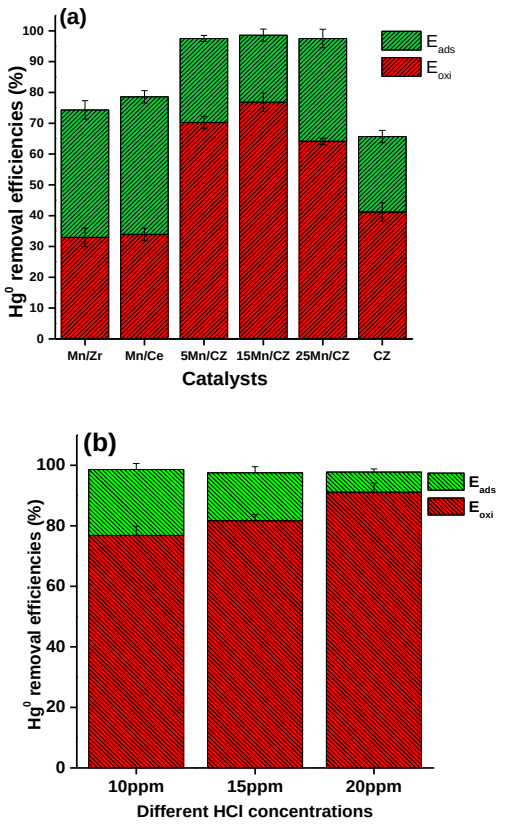

Fig. 7 (a) Hg^0 removal efficiencies of MnO_x/ZrO_2 (Mn/Zr), MnO_x/CeO_2 (Mn/Ce), 5% $MnO_x/Ce_{0.75}Zr_{0.25}O_2$ (5Mn/CZ), 15% $MnO_x/Ce_{0.75}Zr_{0.25}O_2$ (15Mn/CZ), 25% $MnO_x/Ce_{0.75}Zr_{0.25}O_2$

(25Mn/CZ), and $Ce_{0.75}Zr_{0.25}O_2$ (CZ) catalysts. Reaction conditions: 320 µg/m^3 Hg^0, 10 ppm HCl, and N_2 as balance, T=423 K (b) Effect of HCl over 15% $MnO_x/Ce_{0.75}Zr_{0.25}O_2$ (15Mn/CZ) catalyst.

Fig. 7a shows the Hg^0 removal efficiencies (E_{oxi} and E_{ads}) of the different catalysts under a HCl atmosphere at an operating temperature of 423 K. In the presence of HCl (10 ppm), the Mn/Ce, Mn/Zr, and CZ catalysts achieved E_{oxi} in the range of 35–40 %, whereas E_{ads} is in the range of 40–50 %. On the other hand, the Mn/CZ catalysts (5, 15, and 25 % MnO_x) achieved significantly higher E_{oxi} (> 65 %) and lower E_{ads} (> 30 %). In particular, the 15Mn/CZ catalyst achieved the highest E_{oxi} of 76 %.

Furthermore, it was decided to conduct further testing on the influence of HCl concentration on the activity of the best performed catalyst (15Mn/CZ). The results obtained for the aforementioned tests are presented in Fig. 7b. As the concentration of HCl increases from 10 ppm to 20 ppm, the E_{oxi} increased from 76 to 92 %.

3.2.2 Effect of O_2

Recently, there have been increased Hg^0 removal studies over catalysts in the absence of HCl due to a number of coal-fired power plant flue gases containing no or very low concentration of HCl, particularly in the flue gas after WFGD process.[18,19] Hence, the Hg^0 removal efficiency of the catalysts were investigated in the absence of HCl, under 3 % O_2 atmosphere as shown in Fig. 8.

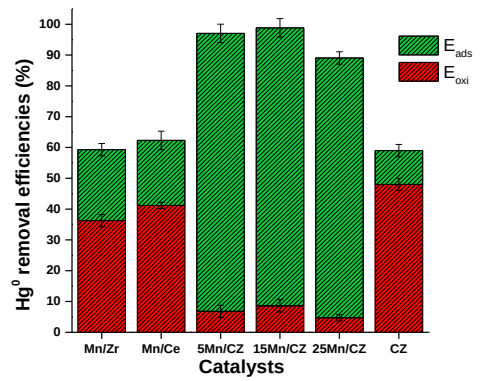

Fig. 8 Hg^0 removal efficiencies of MnO_x/ZrO_2 (Mn/Zr), MnO_x/CeO_2 (Mn/Ce), 5% $MnO_x/Ce_{0.75}Zr_{0.25}O_2$ (5Mn/CZ), 15% $MnO_x/Ce_{0.75}Zr_{0.25}O_2$ (15Mn/CZ), 25% $MnO_x/Ce_{0.75}Zr_{0.25}O_2$ (25Mn/CZ), and $Ce_{0.75}Zr_{0.25}O_2$ (CZ) catalysts. Reaction conditions: 320 µg/m^3 Hg^0, 3 % O_2, and N_2 as balance, T=423 K.

Under 3% of O_2 flue gas conditions, the Mn/Ce, Mn/Zr, and CZ catalysts achieved E_{oxi} values of 38, 35, 41 %, respectively, whereas the 5Mn/CZ, 15Mn/CZ, and 25Mn/CZ catalysts achieved E_{oxi} in the range of 7–10 %. However, the Mn/CZ catalysts show E_{ads} in the range of 75–90 %. The observed low E_{oxi} (high E_{ads}) of Mn/CZ catalysts was most likely due to poor release of HgO from the catalyst surface, thereby indicates that Hg^0 capture was primarily obtained by adsorption. It can be concluded that O_2 has promoted Hg^0 adsorption excessively, but the oxidised mercury exists in the form of HgO, which is in contrast to the HCl atmosphere as shown in Fig. 7a. It is clear that most of Hg^0 species were oxidised by MnO_x during the adsorption process under O_2 atmosphere.[56]

3.2.3 Effect of HCl and O_2

The influence of the presence of HCl and O_2 on gaseous elemental mercury removal was also investigated and the results are shown in Fig. 9. Interestingly, the Mn/CZ catalysts showed more Hg^0 oxidation performances, in particular 15Mn/CZ catalyst show more than 83 % of E_{oxi} among all catalysts. It can be concluded that the presence of O_2 and HCl together played an important role in enhancing Hg^0 oxidation performances. The high concentration of lattice oxygen and/or surface adsorbed oxygen might support the conversion of HCl gas species to active chlorine (Cl*) species. Consequently, the adsorbed Hg^0 reacts with active chlorine species to form HgCl*, thereby $HgCl_2$ species.[22,51] Furthermore, the presence of O_2 could regenerate the consumed oxygen in Hg^0 removal process, hence providing abundant reactive oxygen for reacting with HCl to form enough active Cl* species for Hg^0 oxidation.[57] Compared to O_2 and HCl atmospheres alone (Fig. 7a and Fig. 8), the presence of both gases could transform Hg^0 into $HgCl_2$, which can be easily expelled from the surface of the catalysts at reaction temperature of 423 K. The desorbed $HgCl_2$ species could be easily removed by WFGD technologies due to its high solubility in coal-fired power plants. Therefore, the high Hg^0 removal performance (> 83 % of E_{oxi}) of 15Mn/CZ catalyst suggests the strong interaction between MnO_x and CZ support while compared to Mn/Ce and Mn/Zr catalysts.

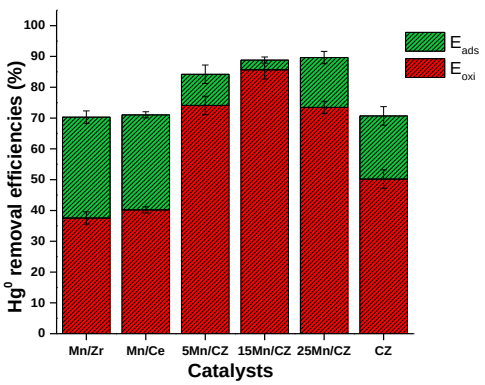

Fig. 9 Hg^0 removal efficiencies of MnO_x/ZrO_2 (Mn/Zr), MnO_x/CeO_2 (Mn/Ce), 5% $MnO_x/Ce_{0.75}Zr_{0.25}O_2$ (5Mn/CZ), 15% $MnO_x/Ce_{0.75}Zr_{0.25}O_2$ (15Mn/CZ), 25% $MnO_x/Ce_{0.75}Zr_{0.25}O_2$ (25Mn/CZ), and $Ce_{0.75}Zr_{0.25}O_2$ (CZ) catalysts. Reaction conditions: 320 µg/m^3 Hg^0, 10 ppm HCl, 3 % O_2, and N_2 as balance, T=423 K

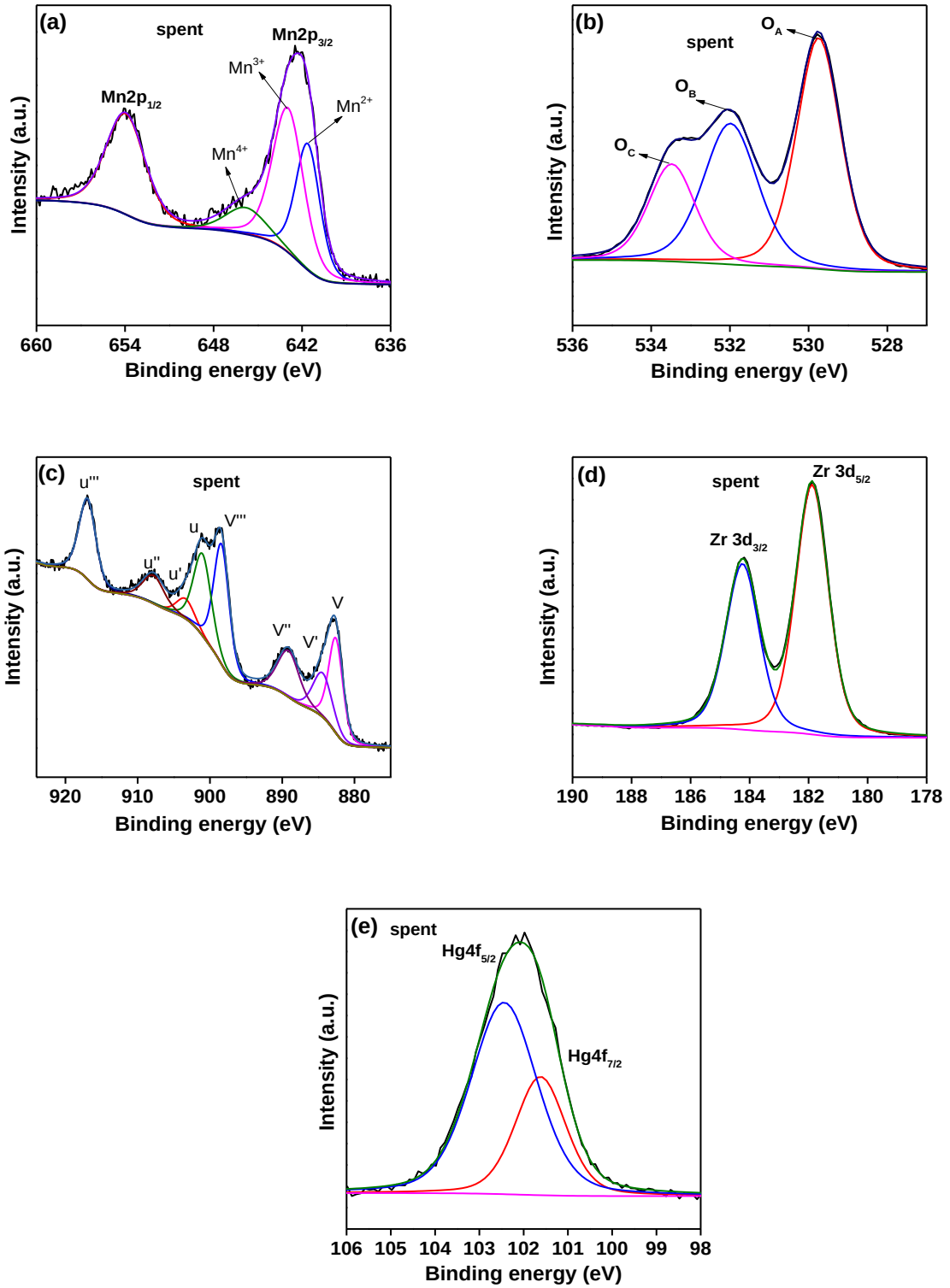

Fig.10 (a) Mn 2p, (b) O 1s, (c) Ce 3d, (d) Zr 3d (e) Hg 4f XPS profiles of spent 15% MnOx/$Ce_{0.75}Zr_{0.25}O_2$ (15Mn/CZ) catalyst after Hg^0 oxidation and adsorption.

3.3 XPS analysis after Hg^0 oxidation and adsorption

XPS analysis of the spent catalysts from the tests performed in the presence of HCl and O_2 (the conditions that gave the highest E_{oxi}) were conducted to investigate if any significant changes occurred on the surface of the catalysts during testing. The XPS profiles of Mn 2p, Ce 3d, O 1s, Zr 3d, and Hg 4f of spent 15Mn/CZ catalyst were shown in Fig. 10. The surface composition ratios of spent 15Mn/CZ catalyst were also illustrated in Table 3.

In Fig. 10 (a), for 15Mn/CZ catalyst, the Mn^{4+} peak intensity decreases, whereas the Mn^{2+} peak intensity increased after Hg^0 removal testing. As observed from Table 3, for 15Mn/CZ catalyst, the ratio of Mn^{4+} decreased from 25.98 to 12.48 %. The more decrease in Mn^{4+} ratio might be enhanced Hg^0 oxidation performances for 15Mn/CZ catalyst (E_{oxi} > 83 %). Moreover, the O 1s XPS spectrum of 15Mn/CZ catalyst was also shown in Fig. 10 (b). After Hg^0 saturation adsorption, the O_C peak intensity increased from 6.3 to 15.4 %, whereas the concentration of O_B decreased from 35.31 % to 32.3 %. Therefore, in this regard, the surface adsorbed oxygen took part in the reaction of Hg^0 oxidation and adsorption. The Ce 3d XPS spectrum of 15Mn/CZ catalyst was also shown in Fig. 10 (c). After Hg^0 adsorption tests, the ratio of $Ce^{4+}/(Ce^{3+}+Ce^{4+})$ decreased from 79.46 to 76.23 %, which indicated the participation of Ce^{4+} in Hg^0 oxidation reactions. The Zr 3d spectrum of 15Mn/CZ catalyst was also shown in Fig. 10 (d). It was clear that Zr 3d spectrum was not changed, thereby confirms the Zr^{4+} did not participate directly in Hg^0 oxidation reaction.

The Hg 4f spectrum of spent 15Mn/CZ catalyst is shown in Fig. 10 (e). The 15Mn/CZ catalyst showed a peak at ~102.3 eV ($Hg4f_{5/2}$), which can be inferred that the Hg^0 is oxidised to HgO, which is adsorbed on the surface of the catalyst.[29,58] A closer analysis of the Hg4f XPS spectrum reveals another deconvoluted peak may be evident at 101.4 eV ($Hg4f_{7/2}$). The appearance of such peak may be attributed to the presence of adsorbed $HgCl_2$ species on the catalyst surface following the Hg^0 oxidation experiments.[59]

3.5 Identification of Hg^0 removal mechanism

The effect of CZ, CeO_2, and ZrO_2 supports on MnO_x dispersion was clearly observed in Hg^0 removal performances and it could be explained through different mechanisms. As observed from the characterization results of fresh and spent catalysts, the active sites like Mn^{4+}/Mn^{3+}, Ce^{4+}/Ce^{3+}, and surface adsorbed oxygen on the catalysts surface were participated in Hg^0 removal reactions. Furthermore, the presence of flue gas conditions changes the E_{oxi} and E_{ads} of catalysts. When in the presence of HCl, Hg^0 removal occurred via catalysts through Langmuir-Hinshelwood mechanism, where the active surface oxygen reacted with adsorbed HCl, thereby forming active chlorine (Cl*).[60] Further the reaction with Cl* and Hg^0 lead to formation of $HgCl_2$. The participation of lattice oxygen and adsorbed surface oxygen was determined from XPS results. The detailed mechanism was explained as follows.

$$2HCl_{(ads)} + [O] \rightarrow 2Cl^* + H_2O \quad (3)$$

$$Hg^0_{(ads)} + Cl^* \rightarrow HgCl^* \quad (4)$$

$$HgCl^* + Cl^* \rightarrow HgCl_{2(ads)} \quad (5)$$

$$HgCl_{2(ads)} \rightarrow HgCl_{2(g)} \quad (6)$$

On the other hand, the presence of HCl and O_2 promoted Hg^0 oxidation, in which the presence of O_2 enhanced the formation of active chlorine species, thereby increased E_{oxi} of 15Mn/CZ catalyst. The Hg^0 oxidation mechanism in presence of HCl and O_2 flue gas are described as follows.

$$HCl_{(g)} \leftrightarrow HCl_{(ads)} \quad (7)$$

$$MnO_2 \rightarrow Mn_2O_3 + [O] \quad (8)$$

$$Mn_2O_3 \rightarrow MnO + [O] \quad (9)$$

$$2CeO_2 \rightarrow Ce_2O_3 + [O] \quad (10)$$

$$[O] + 2HCl_{(ads)} \rightarrow Cl^* + H_2O \quad (11)$$

$$Hg^0_{(ads)} + Cl^* \rightarrow HgCl_{(ads)} \quad (12)$$

$$HgCl_{(ads)} + Cl^* \rightarrow HgCl_{2(ads)} \quad (13)$$

$$2MnO + 1/2O_2 \rightarrow Mn_2O_3 \quad (14)$$

$$Mn_2O_3 + 1/2O_2 \rightarrow 2MnO_2 \quad (15)$$

$$Ce_2O_3 + 1/2O_2 \rightarrow CeO_2 \quad (16)$$

Furthermore, the presence of O_2 conditions alone (absence of HCl) follows the Mars-Maessen mechanism in which the active oxygen from the catalyst directly reacts with adsorbed Hg^0, thereby formation of HgO.[61] The reactions can be represented as follows.

$$Hg^0_{(g)} \rightarrow Hg^0_{(ads)} \quad (17)$$

$$Hg^0_{(ads)} + [O] \rightarrow HgO_{(ads)} \quad (18)$$

Based on the mechanisms and Hg^0 removal results, the Mn/CZ catalysts show higher Hg^0 removal, in particular 15Mn/CZ catalyst exhibit superior catalytic performance. The schematic diagram which explains the conversion of Hg^0 to $HgCl_2$ and/or HgO was shown in Fig. 11. When Zr is incorporated into the CeO_2 lattice, it makes the fluorite structure more defective, thereby forming oxygen vacancies with high mobility at surface, which was strongly supported by Raman and XPS results. The

strong interaction between CZ support and MnO_x also reasoned to enhance Hg^0 removal, which is supported by TPR results. The additional advantage of O_2 in flue gas is that it could oxidize the reduced metal oxides (equations 14 to 16), thereby regenerating active sites (Mn^{4+}, Ce^{4+}, and adsorbed surface oxygen).

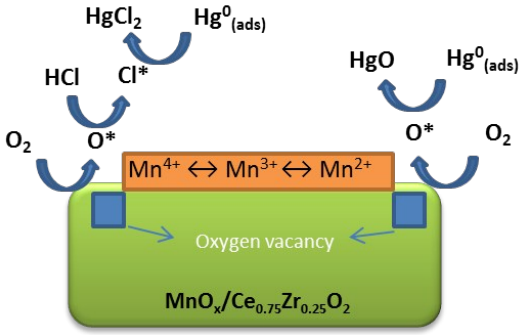

Fig. 11 The schematic representation of Hg^0 oxidation and adsorption mechanism over $MnO_x/Ce_{0.75}Zr_{0.25}O_2$ catalyst.

4. Conclusions

In this work, a series of $yMnO_x/Ce_{0.75}Zr_{0.25}O_2$ (y = 5, 15, and 25 %) catalysts were synthesized by an impregnation method and tested towards Hg^0 removal under simulated flue gas conditions (i.e. presence of HCl and O_2 gas species). The physicochemical properties and Hg^0 removal performances of Mn/CZ catalyst was compared with that of the Mn/Ce, Mn/Zr, and CZ catalysts. It was found that the CZ support enhanced the dispersion of MnO_x nanoparticles, improved the redox properties, and increased the amount of surface adsorbed oxygen thereby significantly enhancing the Hg^0 removal efficiency of MnO_x while compared to CeO_2 and ZrO_2 supported catalysts. In particular, the 15% MnO_x/CZ catalyst was found to reach Hg^0 oxidation efficiencies of up to an impressive ~83 % and removal efficiencies beyond 90%. Furthermore, the Hg^0 oxidation or sorption behaviour was found to be determined by the presence of the flue gas constituents. That is, the presence of HCl or O_2 encouraged Hg^0 oxidation and sorption, respectively. However when both HCl and O_2 were present simultaneously, Hg^0 oxidation efficiency beyond that of presence of O_2 alone was reached with little evidence of Hg^0 sorption occurring. XPS results of the spent 15Mn/CZ catalyst showed that the enhanced Hg^0 removal performance was due to the increased Mn^{4+} density as well as surface adsorbed oxygen during the synthesis process.

Acknowledgements

D. J. would like to acknowledge financial support from RMIT University for providing RMIT-IICT postgraduate scholarship. A. N. and S. K. B would like to thank Deanship for Scientific Research, Visiting Professor Program at King Saud University, for partial support of this work via the Research Group No. RGP-VPP-236.The authors thank the RMMF (RMIT) for providing their comprehensive microscopic facilities for this work and also thank Dr. Ahmad Esmaielzadeh Kandjani for assistance with the XPS measurements.

References

1 C. T. Driscoll, R. P. Mason, H. M. Chan, D. J. Jacob and N. Pirrone, *Environ. Sci. Technol*., 2013, **47**, 4967-4983.
2 L. Zhao, C. Li, X. Zhang, G. Zeng, J. Zhang and Y. e. Xie, *Catal. Sci. Technol*., 2015, **5**, 3459-3472.
3 D. Jampaiah, S. J. Ippolito, Y. M. Sabri, B. M. Reddy and S. K. Bhargava, *Catal. Sci. Technol*., 2015, **5**, 2913-2924.
4 J. He, G. K. Reddy, S. W. Thiel, P. G. Smirniotis and N. G. Pinto, *J. Phys. Chem. C*, 2011, **115**, 24300-24309.
5 D. Jampaiah, K. M. Tur, S. J. Ippolito, Y. M. Sabri, J. Tardio, S. K. Bhargava and B. M. Reddy, *RSC Adv.*, 2013, **3**, 12963-12974.
6 G. K. Reddy, J. He, S. W. Thiel, N. G. Pinto and P. G. Smirniotis, *J. Phys. Chem. C*, 2015, **119**, 8634-8644.
7 X. Weng, R. Mei, M. Shi, Q. Kong, Y. Liu and Z. Wu, *Energy Fuels*, 2015, **29**, 3359-3365.
8 S. Qiao, J. Chen, J. Li, Z. Qu, P. Liu, N. Yan and J. Jia, *Ind. Eng. Chem. Res*., 2009, **48**, 3317-3322.
9 B. M. Reddy, N. Durgasri, T. V. Kumar and S. K. Bhargava, *Catal. Rev*., 2012, **54**, 344-398.
10 Y. Gao, Z. Zhang, J. Wu, L. Duan, A. Umar, L. Sun, Z. Guo and Q. Wang, *Environ. Sci. Technol*., 2013, **47**, 10813-10823.
11 F. Kong, J. Qiu, H. Liu, R. Zhao and Z. Ai, *J. Environ. Sci*., 2011, **23**, 699-704.
12 H. Kamata, S.-i. Ueno, N. Sato and T. Naito, *Fuel Process. Technol*., 2009, **90**, 947-951.
13 X. Zhang, C. Li, L. Zhao, J. Zhang, G. Zeng, Y. e. Xie and M. e. Yu, *Appl. Surf. Sci*., 2015, **347**, 392-400.
14 W. Xiang, J. Liu, M. Chang and C. Zheng, *Chem. Eng. J*., 2012, **200–202**, 91-96.
15 B. Zhang, J. Liu, G. Dai, M. Chang and C. Zheng, *P. Combust. Inst*., 2015, **35**, 2855-286.
16 B. Zhang, J. Liu, C. Zheng and M. Chang, *Chem. Eng. J*., 2014, **256**, 93-100.
17 M. L. Kantam, U. Pal , B. Sreedhar, S. Bhargava, Y. Iwasawa, M. Tada and B. M. Choudary, Adv. Synth. Catal., 2008, **350**, 1225-1229.
18 C. He, B. Shen, J. Chen and J. Cai, *Environ. Sci. Technol*., 2014, **48**, 7891-7898.
19 H. Xu, Z. Qu, C. Zong, W. Huang, F. Quan and N. Yan, *Environ. Sci. Technol*., 2015, **49**, 6823-6830.
20 L. Ji, P. M. Sreekanth, P. G. Smirniotis, S. W. Thiel and N. G. Pinto, *Energy Fuels*, 2008, **22**, 2299-2306.
21 H. Li, C.-Y. Wu, Y. Li and J. Zhang, *Appl. Catal. B*, 2012, **111–112**, 381-388.
22 D. Jampaiah, K. M. Tur, P. Venkataswamy, S. J. Ippolito, Y. M. Sabri, J. Tardio, S. K. Bhargava and B. M. Reddy, *RSC Adv*., 2015, **5**, 30331-30341.
23 J. Li, N. Yan, Z. Qu, S. Qiao, S. Yang, Y. Guo, P. Liu and J. Jia, *Environ. Sci. Technol*., 2010, **44**, 426-431.

24 S. Zhao, Z. Qu, N. Yan, Z. Li, H. Xu, J. Mei and F. Quan, *Catal. Sci. Technol*., 2015, **5**, 2985-2993.

25 D.-W. Jeong, H.-S. Na, J.-O. Shim, W.-J. Jang and H.-S. Roh, *Catal. Sci. Technol*., 2015, **5**, 3706-3713.

26 R. Gao, D. Zhang, P. Maitarad, L. Shi, T. Rungrotmongkol, H. Li, J. Zhang and W. Cao, *J. Phys. Chem. C*, 2013, **117**, 10502-10511.

27 S. Quiles-Diaz, J. Gimenez-Manogil and A. Garcia-Garcia, *RSC Adv*., 2015, **5**, 17018-17029.

28 Y. Li, L. Wang, R. Yan, J. Han and S. Zhang, *Catal. Sci. Technol*., 2015, **5**, 3682-3692.

29 X. Q. Wang, P. Wang, P. Ning, Y. X. Ma, F. Wang, X. L. Guo and Y. Lan, *RSC Adv*., 2015, **5**, 24899-24907.

30 G. Cheng, B. Bai, Q. Zhang and M. Cai, *J. Hazard. Mater*., 2014, **280**, 767-773.

31 S. Kellie, Y. Duan, Y. Cao, P. Chu, A. Mehta, R. Carty, K. Liu, W.-P. Pan and J. T. Riley, *Fuel Process. Technol*., 2004, **85**, 487-499.

32 Y. Xiong, C. Tang, X. Yao, L. Zhang, L. Li, X. Wang, Y. Deng, F. Gao and L. Dong, *Appl. Catal. A*, 2015, **495**, 206-216.

33 B. M. Reddy, G. Thrimurthulu, L. Katta, Y. Yamada and S.-E. Park, *J. Phys. Chem. C*, 2009, **113**, 15882-15890.

34 P. Venkataswamy, D. Jampaiah, F. Lin, I. Alxneit and B. M. Reddy, *Appl. Surf. Sci*., 2015, **349**, 299-309.

35 Z. Ma, X. Wu, Z. Si, D. Weng, J. Ma and T. Xu, *Appl. Catal. B*, 2015, **179**, 380-394.

36 B. M. Reddy, P. Saikia, P. Bharali, L. Katta and G. Thrimurthulu, *Catal. Today*, 2009, **141**, 109-114.

37 M. Guo, J. Lu, Y. Wu, Y. Wang and M. Luo, *Langmuir*, 2011, **27**, 3872-3877.

38 A. Chen, Y. Zhou, N. Ta, Y. Li and W. Shen, *Catal. Sci. Technol*., 2015, **5**, 4184-4192.

39 B. M. Reddy, A. Khan, Y. Yamada, T. Kobayashi, S. Loridant and J.-C. Volta, *J. Phys. Chem. B*, 2003, **107**, 11475-11484.

40 T. Taniguchi, T. Watanebe, S. Ichinohe, M. Yoshimura, K.-i. Katsumata, K. Okada and N. Matsushita, *Nanoscale*, 2010, **2**, 1426-1428.

41 J.-R. Kim, W.-J. Myeong and S.-K. Ihm, *J. Catal*., 2009, **263**, 123-133.

42 R. Si, Y.-W. Zhang, S.-J. Li, B.-X. Lin and C.-H. Yan, *J. Phys. Chem. B*, 2004, **108**, 12481-12488.

43 J. Zuo, Z. Chen, F. Wang, Y. Yu, L. Wang and X. Li, *Ind. Eng. Chem. Res*., 2014, **53**, 2647-2655.

44 D. Jampaiah, P. Venkataswamy, K. M. Tur, S. J. Ippolito, S. K. Bhargava and B. M. Reddy, *Zeitschrift für anorganische und allgemeine Chemie*, 2015, **641**, 1141-1149.

45 B. Shen, Y. Wang, F. Wang and T. Liu, *Chem. Eng. J*., 2014, **236**, 171-180.

46 J. Xie, Z. Qu, N. Yan, S. Yang, W. Chen, L. Hu, W. Huang and P. Liu, *J. Hazard. Mater*., 2013, **261**, 206-213.

47 Y. Adnan, C. Dewei and L. Sean, *J. Phys. D: Appl. Phys*., 2012, **45**, 355101.

48 S. Xie, H. Dai, J. Deng, Y. Liu, H. Yang, Y. Jiang, W. Tan, A. Ao and G. Guo, *Nanoscale*, 2013, **5**, 11207-11219.

49 Z. Wu, R. Jin, Y. Liu and H. Wang, *Catal. Commun*., 2008, **9**, 2217-2220.

50 H. Li, C.-Y. Wu, Y. Li and J. Zhang, *Environ. Sci. Technol*., 2011, **45**, 7394-7400.

51 P. Venkataswamy, K. N. Rao, D. Jampaiah and B. M. Reddy, *Appl. Catal. B*, 2015, **162**, 122-132.

52 Y. Yu, L. Zhong, J. Ding, W. Cai and Q. Zhong, *RSC Adv*., 2015, 5, 23193-23201.

53 D. Fang, J. Xie, H. Hu, H. Yang, F. He and Z. Fu, *Chem. Eng. J*., 2015, **271**, 23-30.

54 Z. Liu, H. Su, J. Li and Y. Li, *Catal. Commun*., 2015, **65**, 51-54.

55 M. Daturi, E. Finocchio, C. Binet, J.-C. Lavalley, F. Fally, V. Perrichon, H. Vidal, N. Hickey and J. Kašpar, *J. Phys. Chem. B*, 2000, **104**, 9186-9194.

56 H. Li, C.-Y. Wu, Y. Li, L. Li, Y. Zhao and J. Zhang, *J. Hazard. Mater*., 2012, **243**, 117-123.

57 Y. Li, P. D. Murphy, C.-Y. Wu, K. W. Powers and J.-C. J. Bonzongo, *Environ. Sci. Technol*., 2008, **42**, 5304-5309.

58 H. Li, S. Wu, C.-Y. Wu, J. Wang, L. Li and K. Shih, *Environ. Sci. Technol*., 2015, **49**, 7373-7379.

59 J. Zheng, F. Li, X. Yu, C.-H. Huang and N. Wu, *Phys. Chem. Chem. Phys*. 2000, **2**, 3049-3053.

60 B. Zhang, J. Liu, Y. Yang and M. Chang, *Chem. Eng. J*., 2015, **280**, 354-362.

61 A. A. Presto and E. J. Granite, *Environ. Sci. Technol*., 2006, **40**, 5601-5609.

TOC Graphic

The developed ceria-zirconia modified MnO_x catalysts were found to have enhanced Hg^0 oxidation and removal performance.